Tribology International Vol. 31, No. 8, pp. 425–433, 1998

Printed in Great Britain
0301–679X/98/$19.00 + 0.00

PII: S0301–679X(98)00064–4

Atomic scale deformation in silicon monocrystals induced by two-body and three-body contact sliding

Liangchi Zhang* and Hiroaki Tanaka†

This paper discusses the deformation of silicon monocrystals subjected to two-body and three-body contact sliding with the aid of the molecular dynamics analysis. It was found that amorphous phase transformation is the main deformation in silicon and the onset of such inelastic deformation can be well predicted by a stress criterion. In a two-body contact sliding, the deformation of silicon falls into no-wear, adhering, ploughing and cutting regimes, while in a three-body contact sliding it follows the regimes of no-wear, condensing, adhering and ploughing. Under certain conditions in three-body sliding, wear without any subsurface damage can also occur when the bonding strength among surface silicon atoms is weakened and material removal takes place through the mechanism of adhesion. Based on the detailed deformation analysis, a new friction law and a new concept for wearability evaluation were proposed.

Keywords: *silicon monocrystal, contact sliding, amorphous phase change, stress criterion, wear and friction*

Introduction

When two surfaces are in contact sliding without foreign particles, they are in two-body contact sliding. In this case, the interactions among surface asperities play a central role in the process of wear and friction. If some particles appear between the surfaces, which could be the debris from worn surfaces or foreign particles due to contamination, a three-body contact sliding occurs. Under such circumstances, the kinetics and properties of the particles contribute to the tribology of the surfaces. The above sliding processes are common in nanotribological systems.

This paper aims to gain an understanding of the friction and wear mechanisms in silicon associated with a two-body or a three-body contact sliding. Emphasis will be placed on the subsurface deformation in a sliding component. As the research interest is on the atomic and nanometre scales, the molecular dynamics method[1–3] will be used as a theoretical tool in conjunction with a corresponding experimental analysis.

Method

Modelling

In a two-body contact sliding, as shown in Fig 1(a), asperities are fixed on the sliding surfaces. To understand the fundamental deformation mechanism in a component induced by the penetration of asperities, it is necessary to first investigate the deformation of a smooth silicon surface subjected to the sliding of a single asperity. The mechanics model is illustrated in Fig 1(b), where the shape of a hard asperity, which should be irregular in reality, has been simplified to a

†*Current address: Dept of Precision Engineering, Faculty of Engineering, Osaka Electro-Communication University, 18-8 Hatsu-cho, Neyagawa, Osaka 572, Japan*
Department of Mechanical and Mechatronic Engineering, The University of Sydney, Sydney, NSW 2006, Australia
**Corresponding author. Tel: + 61-2-9351-2835; Fax: + 61-2-9351-3760; E-mail: zhang@mech.eng.usyd.edu.au*

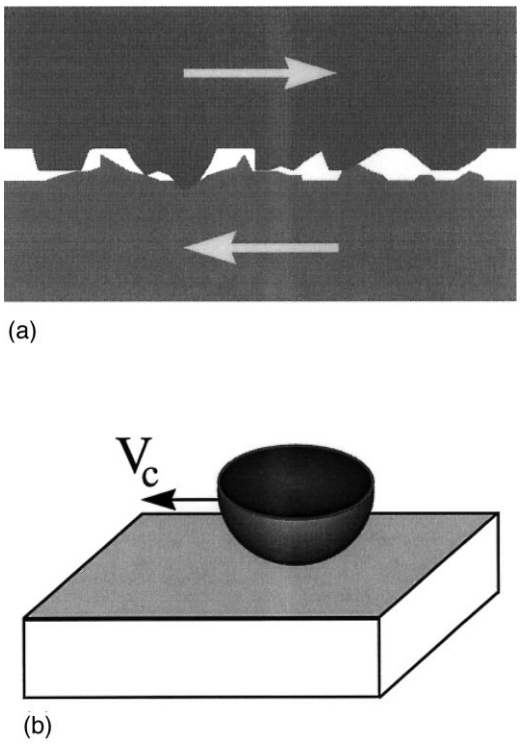

Fig. 1 Modelling of a two-body contact sliding process, (a) sliding of surfaces with asperities, (b) a simplified model

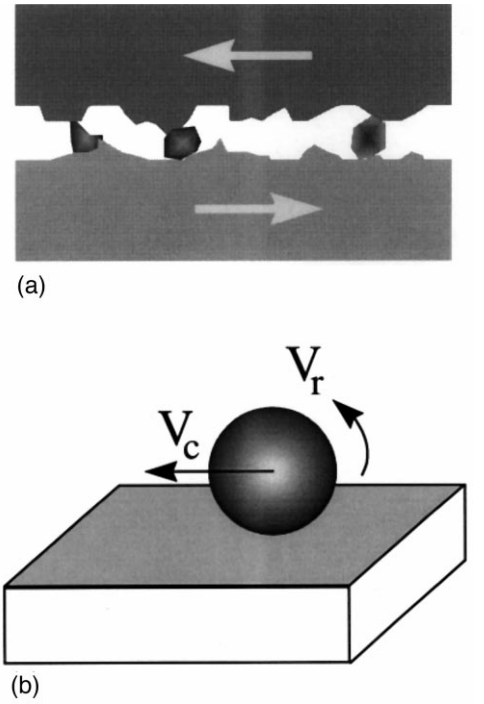

Fig. 2 Modelling of a three-body contact sliding process, (a) sliding of surfaces with free particles, (b) a simplified model

hemispherical diamond tip of radius R moving with a constant speed V_c. Since a diamond can be considered as a rigid body compared with silicon, the model enables one to concentrate on the understanding of deformation of silicon. In a three-body contact sliding, as illustrated in Fig 2(a) however, the motion of a foreign particle between the two surfaces possesses both a translation and a self-rotation. To facilitate understanding, again, a single particle is considered and is approximated by a diamond ball of radius R, moving horizontally (translation) with a speed V_c and in the meantime rotating about its centre independently with a peripheral speed V_r, as shown in Fig 2(b). When $V_r = 0$, the three-body contact sliding becomes a two-body one. When $V_c = 0$ or $V_r = V_c$, on the other hand, it becomes a pure rolling process.

The mechanics models in Fig 1(b) and Fig 2(b) can be used in molecular dynamics analysis, as shown in Fig 3. To avoid the boundary effect, the dimension of the moving control volume[1,2] (MCV) of a silicon specimen was taken as 9.23 nm × 13.57 nm × 4.34 nm, containing 28 773 silicon atoms. To eliminate the rigid body motion of the specimen and guarantee a reasonable heat conduction outwards the MCV, layers of boundary atoms, which are fixed to the space, and layers of thermostat atoms, which absorb the heat at the MCV boundaries, are arranged[1–3] to surround the Newtonian atoms of silicon in the MCV except its top surface that is subjected to asperity/particle sliding. According to the atomic structure of silicon, Tersoff potential[4] was used to describe the interactions among silicon atoms and Morse potential[2] was employed to reflect those among silicon and diamond atoms. Based on a careful investigation[3], it was found that the most suitable equations for temperature conversion from the kinetic energy of an atom are the Debye equation for silicon and Einstein equation for diamond. These equations were therefore used correspondingly in the present temperature conversion.

As can be seen more clearly later both theoretically and experimentally, variation of deformation mechanisms happens before the indentation depth of an asperity/particle reaches 1 nm. In addition, dislocations do not appear when the indentation depth is below a few nanometres. Thus the dimension of MCV selected above is sufficiently large and is optimum in terms of calculation efficiency.

Experiment

Experimental investigations were also carried out in two ways, i.e., in two-body and three-body contact sliding, to examine the variations of surface and subsurface microstructures of silicon monocrystals with sliding conditions and to understand and verify the theoretical predictions of molecular dynamics analysis. The two-body sliding experiment was performed on a modified ultra-precision surface grinder, Minini Junior CNC M826, by mounting silicon specimens on the table and diamond asperity tips on a disk that was fixed on the machine spindle*. The three-body sliding was conducted on a precision polishing machine so

**In this way, a high speed sliding can be carried out when varying the rotation speed of the disk. An associated approximation with such an experimental set-up is the non-uniform penetration depth of the asperity. The penetration depth given in the experimental figures below are the maximum depth correspondingly.*

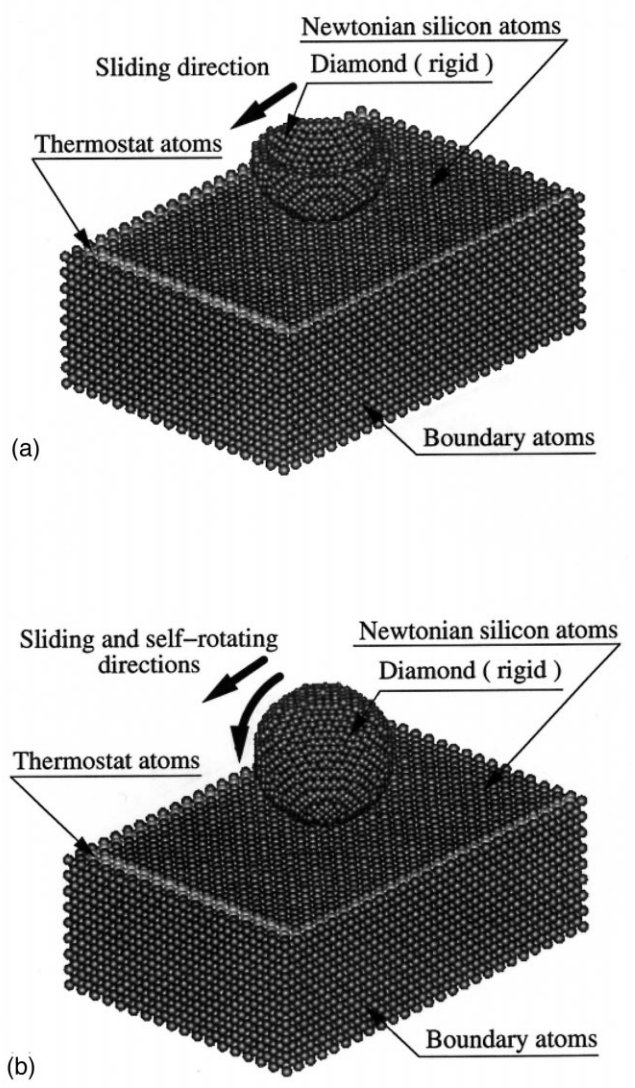

Fig. 3 Molecular dynamics modelling of the sliding processes, (a) a two-body contact sliding, (b) a three-body contact sliding

that slurry foreign particles can be added into the interface of the sliding surfaces. The subsurface structure was investigated by a Transmission Electron Microscope, EM430, and a Scanning Transmission Electron Microscope, VGHB601.

Results and discussion

Inelastic deformation

Both the theoretical and experimental results showed that there always exists a thin layer of amorphous silicon in a specimen subsurface subjected to a two-body contact sliding, as shown in Fig 4(a) to (c). The thickness of the layer decreases with decreasing the penetration depth of asperity (Fig 4(d)), δ. If δ is large (e.g., 763 nm), two dislocation systems, (111)[101] and (111)[011], can be developed in the crystal silicon below the amorphous layer. When δ becomes smaller (e.g., 15.2 nm), only one dislocation system, (111)[$10\bar{1}$], appears (Fig 4(c))*. If δ decreases further, dislocations cannot be activated but the amorphous layer still appears. This means that on the nanometre scale an inelastic deformation via amorphous phase transformation is an energetically more favourable mechanism than that via the evolution of dislocations. In the case with three-body contact sliding, the mechanism of inelastic deformation is the same, i.e., via viscous flow in the amorphous zone. However, because of the kinetic difference in the two-body and three-body sliding motions, the extent of subsurface damage is different. In general, a two-body contact sliding introduces a thinner layer of amorphous. A three-body contact sliding, however, may leave a perfect crystal structure after sliding although wear has happened, see Fig 5, depending on the penetration depth of the particle, its speed ratio of self-rotation to translation and variation of atomic bonding strength affected by surface contamination. It was also found that the variation of sliding velocity from 20 m/s to 200 m/s does not change the deformation mechanisms described above.

The deformation of a silicon monocrystal under a two-body or a three-body contact sliding thus has the following distinct features:

(a) Phase transformation, from the original crystal to amorphous, happens shortly after the asperity/particle penetration.

(b) Wear always takes place within the amorphous layer regardless of the appearance of dislocations in the crystal region. In other words, the mechanism of material removal is due to the viscous flow inside the amorphous zone. When δ is below 763 nm, no microcracks have been initiated.

(c) Re-crystallisation occurs in the amorphous layer behind an asperity/particle, from the bottom of the layer to the surface. As a result, the residual amorphous layer is always thinner or even disappears.

(d) Under the same penetration depth, three-body contact sliding introduces a deeper subsurface damage.

Wear regimes

Wear regimes depend on sliding conditions, as shown by the mechanism diagram, Fig 6. In a two-body contact sliding with a given sliding speed, the deformation of a silicon monocrystal falls into *no-wear*, *adhering*, *ploughing* or *cutting* regime when the asperity penetration depth varies, see the left half of Fig 6. These wear regimes are similar to those in the contact sliding of metals on the nanometre scale[2]. Deformation without wear happens only under an extremely small penetration depth, when the atomic lattice of silicon deforms purely elastically. With increasing the penetration depth, adhering takes place

**Note that to reveal the dislocation structure on the cross-section shown in Fig 4(c), the TEM beam cannot be perpendicular to the specimen surface. Thus the amorphous layer in the photograph does not show its actual thickness. Fig 4(d) gives the true thicknesses of amorphous layers that were measured by a beam perpendicular to specimen surfaces.*

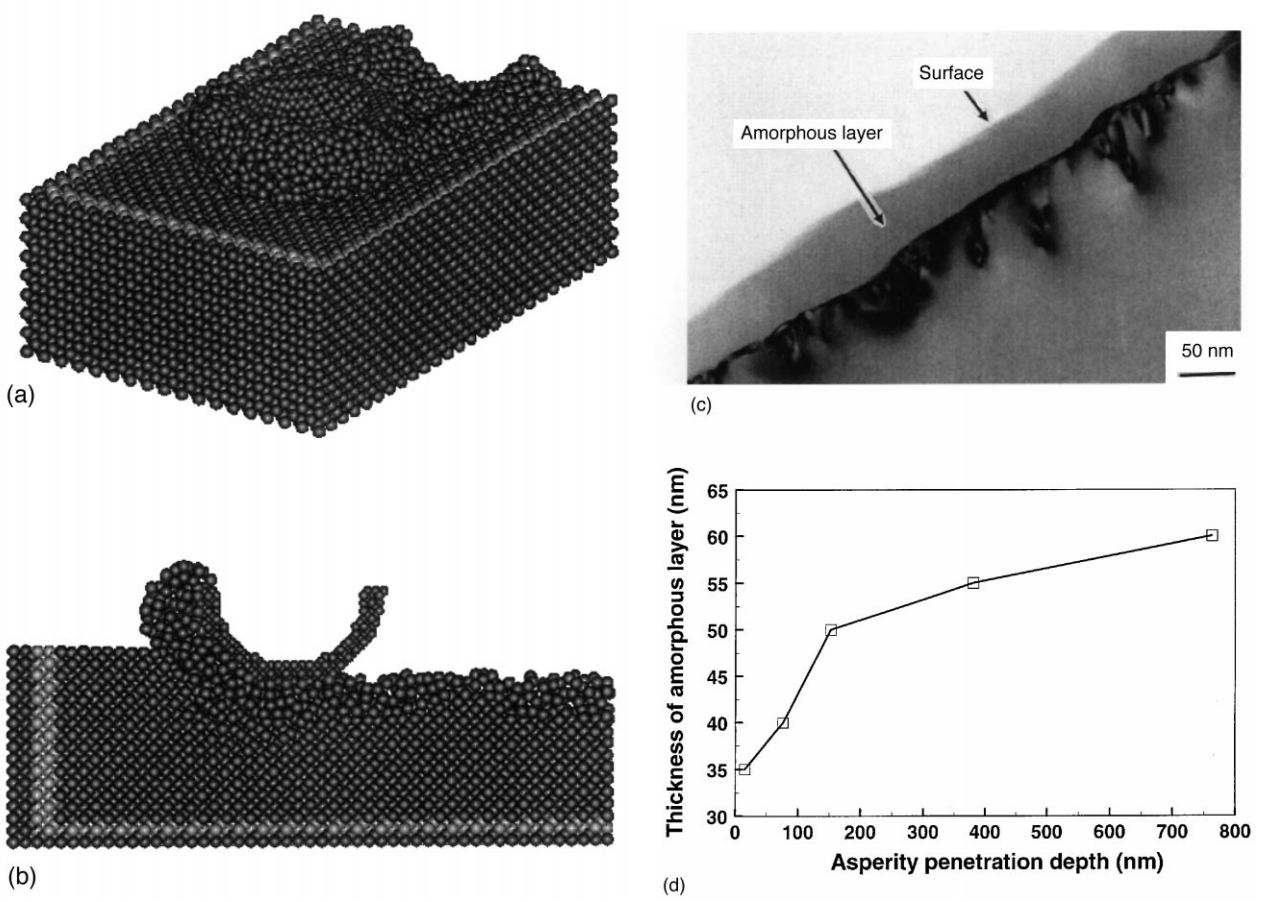

Fig. 4 The subsurface microstructure of silicon monocrystals after a two-body contact sliding. The diamond asperity is moving from the right to the left in (a) and (b). (a) The amorphous phase transformation predicted by the three-dimensional molecular dynamics analysis (V_c = 200 m/s, R = 2.1 nm, δ = 0.99 nm, sliding in [100] direction); (b) a cross-sectional view of the deformed subsurface of the specimen shown in (a); (c) an experimental result of the subsurface damage induced. Note the top amorphous layer and the dislocations in the crystal zone (V_c = 23.95 m/s, R = 1 μm, δ = 15.2 nm, sliding in [100] direction); (d) experimental observation on the thickness variation of amorphous layer with asperity indentation depth (V_c = 23.95 m/s, R = 1 μm, sliding in [100] direction)

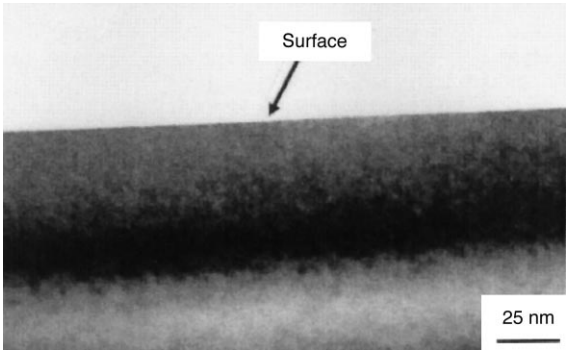

Fig. 5 A perfect crystal subsurface in a specimen after a three-body contact sliding (R = 12.5 nm). The thickness of the surface layer removed was 1.25 μm

(Fig 7(a) and (b)). In this case, some surface atoms stick to the asperity surface and move together with it to cause wear. However, these atoms may return to the silicon substrate during sliding if the specimen surface has not been contaminated. When the penetration depth increases further, a new wear state, ploughing, characterised by an atomic cluster being pushed to move with the asperity, will appear (Fig 7(c) and (d)). A further increase of the penetration depth leads to a continuous cutting process (Fig 4(a) and (b)).

In a three-body contact sliding, however, a silicon specimen will experience different wear regimes. They are the *no-wear*, *condensing*, *adhering* and *ploughing* regimes, as shown in the right half of Fig 6. After the pure elastic deformation in the no-wear regime, the amorphous phase under the particle will experience a remarkable condensing locally without material removal. In other words, because the density of the surface silicon atoms under particle indentation becomes higher, condensing creates a sliding mark on the specimen surface, see Fig 8(a). Thus condensing is a special wear process without material removal. A further particle penetration will lead to adhering and ploughing (Fig 8(b) to (c)). These regimes are similar to the corresponding ones in the two-body contact sliding. Cutting rarely happens in three-body sliding processes but is possible if the particle penetration

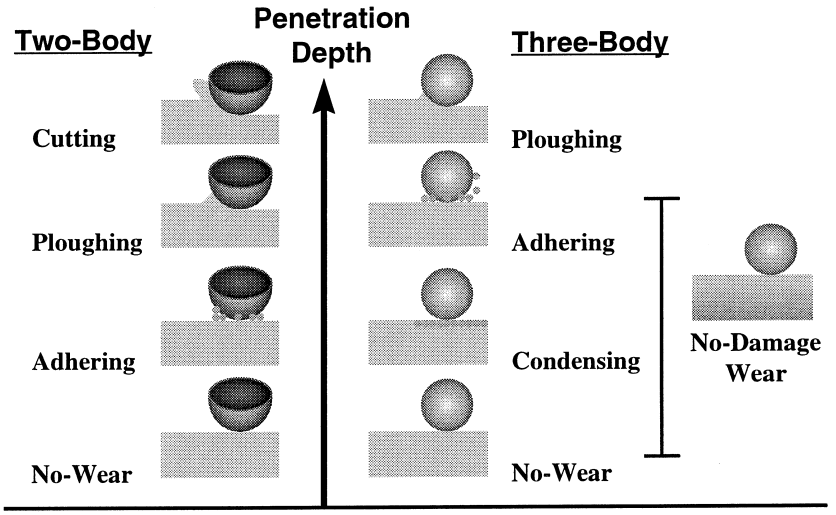

Fig. 6 The wear diagram. The diamond asperities/particles move from the right to the left. The rotation of particles is anticlockwise

depth becomes sufficiently large and the self-rotation speed becomes small.

Another interesting phenomenon associated with the three-body contact sliding is the existence of a regime of *no-damage wear*, as shown in Fig 5. Under certain sliding conditions, the atomic bonding strength among surface silicon atoms can be weakened chemically[5,6]. When the bonding weakening happens, these atoms can be removed via adhesion because diamond–silicon attraction is still strong, as illustrated in Fig 9*. Due to the re-crystallisation behind the particle, a worn specimen may appear as damage-free in the majority of its subsurface with only little distortion within one or two surface atomic layers (Figs 5 and 9). In conjunction with the phenomenon happening in the condensing regime discussed above, it becomes obvious that a perfect subsurface after a three-body contact sliding does not necessarily indicate a no-wear process.

Prediction of phase change

It is now clear that amorphous phase transformation plays a central role in the wear of a silicon specimen. Thus a natural question is how to conveniently predict the onset of such inelastic deformation. This, like the prediction of initial yielding in a metal, is of primary importance to the design, fabrication and application of a silicon component.

In a recent investigation into the nano-indentation of silicon, Zhang and Tanaka[3] showed that the onset of amorphous transformation can be predicted by their octahedral shear stress criterion, which states that when

$$\frac{1}{3}\sqrt{(\sigma_1-\sigma_2)^2+(\sigma_2-\sigma_3)^2+(\sigma_3-\sigma_1)^2} = \tau_c^{oct} \quad (1)$$

holds, amorphous transformation takes place, where τ_c^{oct} is the threshold of octahedral shear stress at the onset of amorphous change and was found to be 4.6 GPa to 7.6 GPa in indentation depending on directions due to the anisotropy of silicon. This criterion is based on the argument that amorphous change in crystal silicon is induced by the severe atomic lattice distortion under a complex three-dimensional stress field that breaks the original atomic bonding among silicon atoms.

Using the method of stress calculation developed by Zhang and Tanaka[3], the octahedral shear stress can be examined over the whole control volume, see for example, Fig 10. The results immediately lead to the conclusion that an amorphous transformation in the loading zone occurs when the octahedral shear stress reaches 4.6 GPa in direction [100] and 7.6 GPa in direction [110]. This is in exact agreement with the τ_c^{oct} in indentation[3]. The octahedral shear stress criterion thus can also predict very well the onset of amorphous change in both the two-body and three-body contact sliding processes. A more accurate prediction needs the development of a criterion that can accommodate the anisotropy of silicon.

The octahedral shear stress criterion is similar to the von Mises for an initial plastic yielding of a metal except the different origin of τ_c^{oct}. One therefore may immediately think that the Tresca yielding function for metals may also bring about a good prediction. An investigation shows that it is also usable provided that the threshold of the maximum shear stress at the onset of amorphous, τ_c^{max}, be taken as 5.3 GPa in direction [100] to 10.3 GPa in direction [110]. However, the maximum shear stress criterion gives less accurate profile prediction of the amorphous zone.

Based on the experimental observations of Hu *et al.*[8] under hydrostatic conditions, Pharr *et al.*[7] concluded that the formation mechanism of amorphous in nano-indentation was due to the hydrostatic stress component. Amorphous change occurred when indentation generated a sufficiently large hydrostatic stress. Wep-

**To facilitate the molecular dynamics simulation, it was assumed in Fig 9 that the effect of the weakened Si–Si interactions can be qualitatively reflected by the stronger C–Si interactions while keeping the Si–Si bonding strength unchanged.*

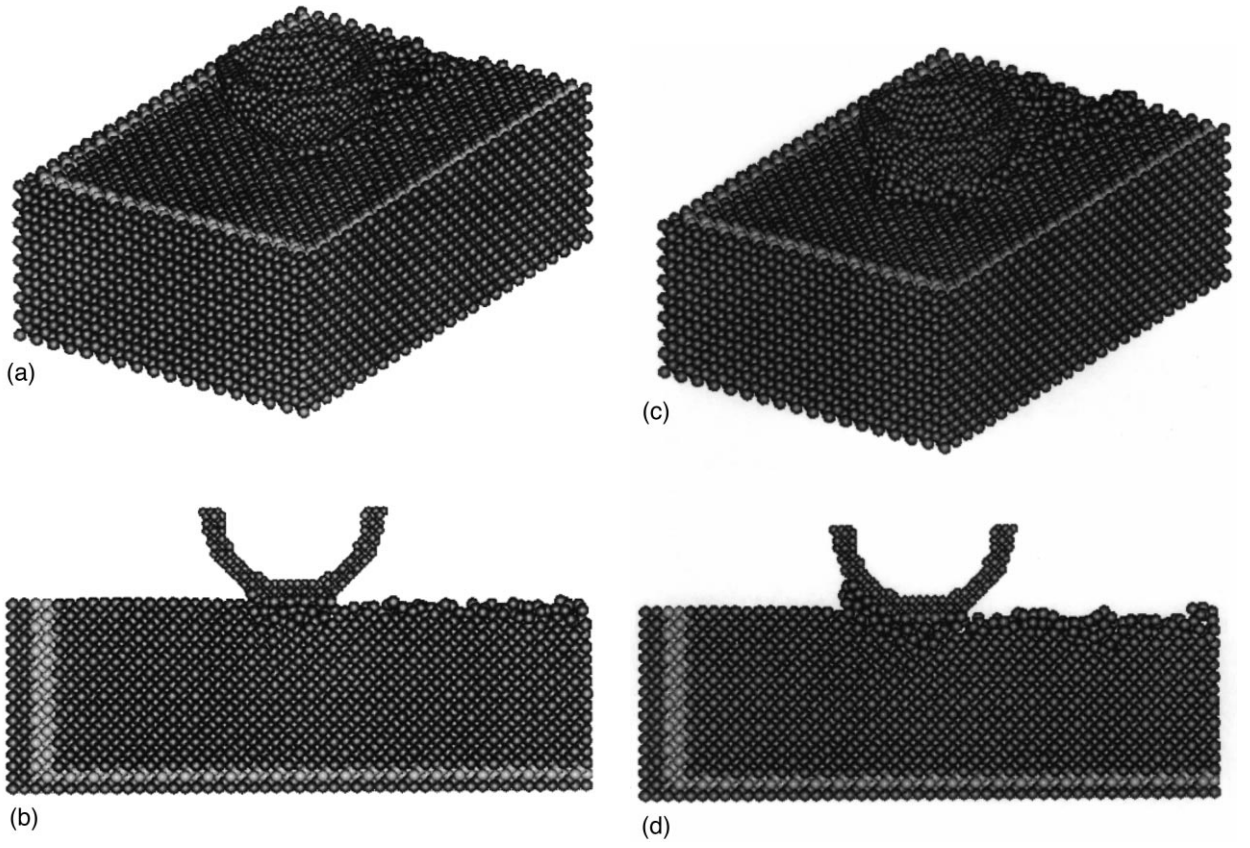

Fig. 7 Characteristics of various deformation regimes in two-body contact sliding processes. The sliding conditions are V_c *= 200 m/s,* R *= 2.1 nm, sliding in [100] direction and* δ *= 0.19 nm for (a) and (b) and* δ *= 0.39 nm for (c) and (d). The asperity is moving from the right to the left. (a) adhering—a three-dimensional view, (b) adhering—a cross-sectional view, (c) ploughing—a three-dimensional view, (d) ploughing—a cross-sectional view*

pelmann *et al*.[9] also concluded that the hydrostatic stress at the onset of transformation during loading was 11.3 GPa and at the reverse transformation during unloading was 8.4 GPa, which were almost identical with the values measured by Hu *et al*.[8] (11.3–12.5 GPa during pure hydrostatic loading and 8.5–10.8 GPa during pure hydrostatic unloading). Nevertheless, these conclusions were based on the maximum hydrostatic stress at a given indentation load, which overlooked the difference between the onset of amorphous phase and the development of an existing amorphous zone, and ignored the dependence of such inelastic deformation on loading history. If the hydrostatic stress, with the threshold of 11.3 GPa, is used to measure the onset of phase change in the loading zones in two-body and three-body contact sliding processes, it can be seen easily from Fig 11 that the predicted amorphous zones will be much smaller than what they should be. An error will also occur in the unloading zones if the threshold of 8.5 GPa is applied. A similar conclusion was also obtained by Zhang and Tanaka[3] in indentation. It is therefore clear that hydrostatic stress does not provide a correct measure for the onset of amorphous transformation in either indentation or contact sliding.

Friction

When the penetration depth is very small, i.e., when the deformation of silicon falls into the regime of no-wear, condensing, or adhering*, the conventional definition of friction coefficient becomes inappropriate to describe the frictional behaviour, since a singularity appears, as shown in Fig 12. Thus experimentally, one may find that the repeatability of a measured friction coefficient is low when the sliding condition falls into one of these regimes. The singularity is caused by the transition of the normal sliding force, F_z, from tensile to compressive as shown in Fig 13, which is a common phenomenon in nano-sliding systems[2]. In the regime of ploughing or cutting, the friction coefficient keeps almost constant and the effect of the type and direction of sliding is invisible. This is because ploughing and cutting take place within amorphous zones and the resistance to viscous flow deformation does not vary considerably.

It is now clear that the frictional behaviour should be described individually according to sliding conditions. In ploughing and cutting regimes, the conventional friction law, i.e., $F_x = \mu F_z$, still applies on the nanometre scale, where μ is a constant friction coefficient. In no-wear, condensing and adhering regimes, however, a new law must be derived. Fig 14 shows that the frictional force, F_x, is a function of the contact area and obeys a simple power law, i.e.,

*$\delta < 0.3$ nm for two-body sliding and $\delta < 0.5$ nm for three-body sliding.

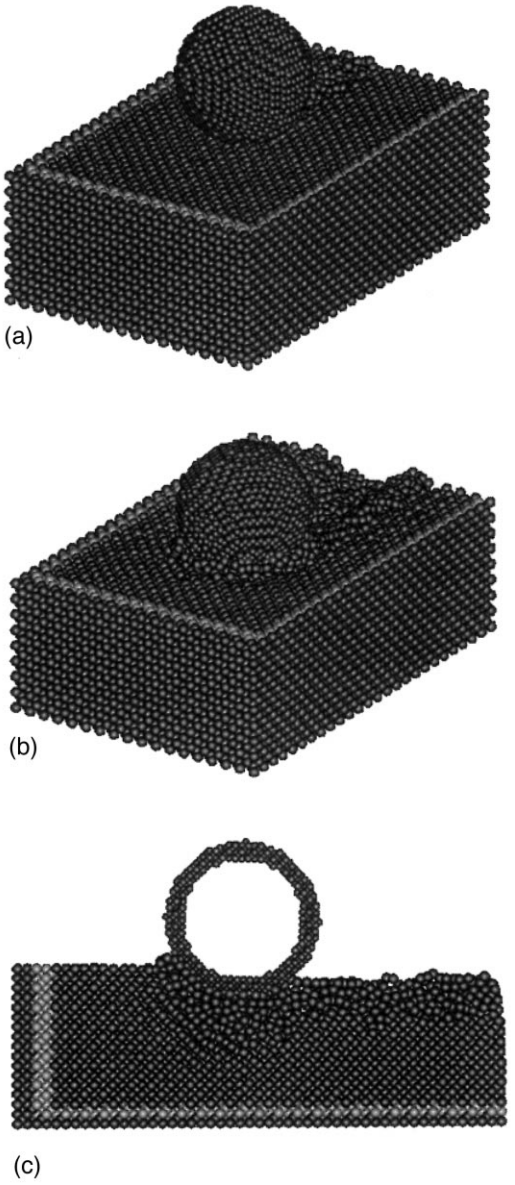

Fig. 8 Deformation regimes associated with three-body contact sliding. V_c *= 200 m/s,* V_r *= 100 m/s,* R *= 2.1 nm, sliding in [100] direction and* δ *= 0.19 nm for (a) and* δ *= 0.99 nm for (b) and (c). The particle translation is from the right to the left and its rotation is anticlockwise. (a) condensing, (b) ploughing—a three-dimensional view, (c) ploughing—a cross-sectional view*

$$F_x = k(A^c_{\text{atomic}})^{\xi} \quad (2)$$

where the A^c_{atomic} is the contact area calculated by the atomic approach defined by Zhang and Tanaka[3] and k and ξ are constant factors. Equation (2) is valid for both the two-body and three-body contact sliding processes and is independent of sliding directions. It is very interesting to note that the frictional force in the ploughing regime can be described by both the friction laws. Thus ploughing can be regarded as a transition regime when friction is concerned.

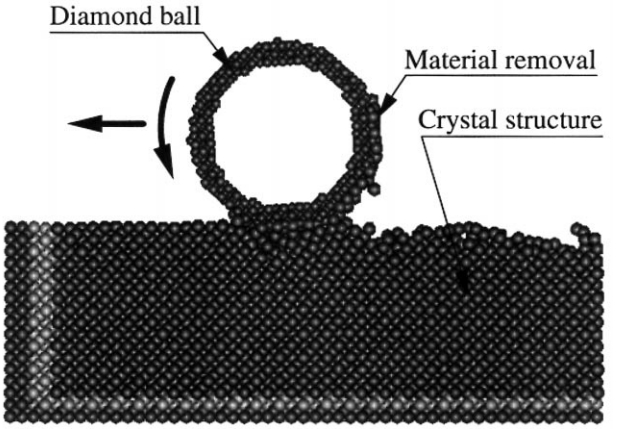

Fig. 9 Material removal via adhering in a three-body sliding process when the C–Si interaction is three times stronger than that of Si–Si. The particle translation is from the right to the left and its rotation is anticlockwise. (V_c *= 200 m/s,* V_r *= 100 m/s,* R *= 2.1 nm and* δ *= 0.19 nm)*

Wearability

To evaluate the wearability of silicon under different sliding conditions, it is convenient to introduce the concept of *specific energy of wear*, which is defined as the frictional energy per unit volume of material removal. Thus under a given sliding condition, a material with a greater specific energy has a higher wearability. With a given material, however, a greater specific energy under certain sliding conditions means a higher wearability against these sliding conditions. Fig 15 is an example demonstrating the variation of wearability of silicon monocrystals against sliding speed and asperity penetration depth in two-body sliding processes. It shows that increasing the sliding speed or penetration depth lowers the specific energy of wear and thus reduces the wearability, since a larger V_c or δ will generate a greater temperature rise, increase the deformability of the amorphous silicon and decrease the specific energy of wear.

Conclusions

The following conclusions can be drawn according to the above analysis:

1. The wear of silicon monocrystals on the nanometre scale is due to the deformation via viscous flow within the amorphous layer. Associated with a two-body contact sliding, there exist no-wear, adhering, ploughing and cutting regimes, while with a three-body contact sliding there are five regimes, which are no-wear, condensing, adhering, ploughing and no-damage wear regimes.
2. Dislocations are not important to the sliding wear of a silicon monocrystal on the atomic scale. Deformation via amorphous phase transformation and its associated viscous flow is more favourable than that via the evolution of dislocations.
3. The octahedral shear stress criterion can be used to predict the onset of amorphous transformation in both the two-body and three-body sliding pro-

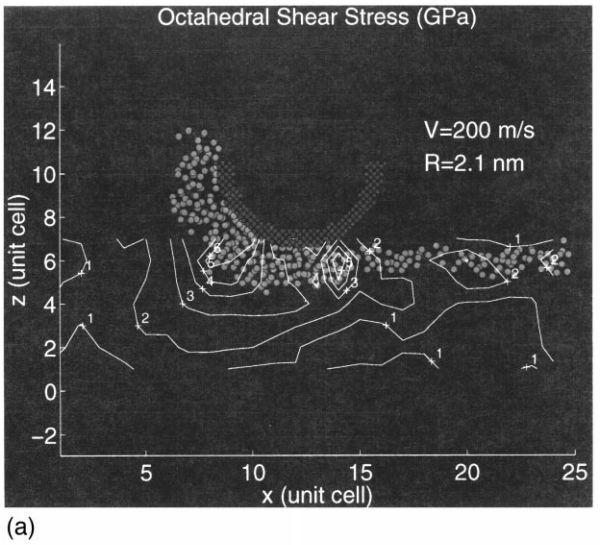

Fig. 10 Octahedral shear stresses in silicon specimens subjected to sliding. The particle translation is from the right to the left and its rotation is anticlockwise (V_c = 200 m/s, V_r = 100 m/s, R = 2.1 nm, δ = 0.99 nm). (a) Two-body contact sliding, (b) three-body contact sliding

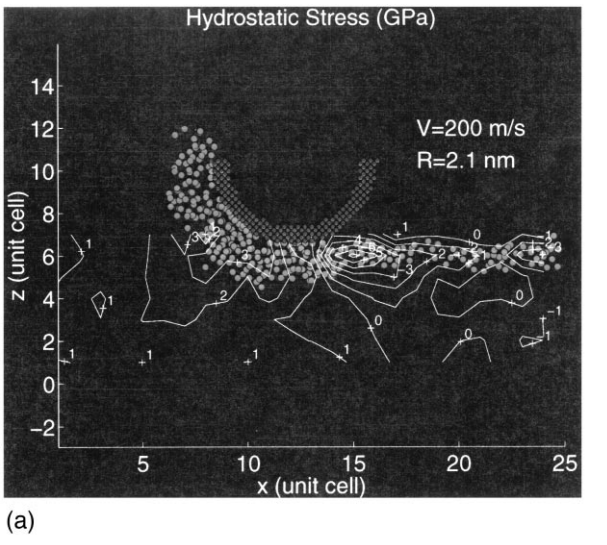

Fig. 11 Hydrostatic stresses in silicon specimens subjected to sliding. The particle translation is from the right to the left and its rotation is anticlockwise (V_c = 200 m/s, V_r = 100 m/s, R = 2.1 nm, δ = 0.99 nm). (a) Two-body contact sliding, (b) three-body contact sliding

cesses with the threshold of τ_c^{oct} = 4.6 GPa to 7.6 GPa, depending on sliding directions. The τ_c^{oct} is in agreement with that in nano-indentation.

4. Two friction laws are needed to describe the frictional behaviour of silicon monocrystals subjected to contact sliding, i.e.,

$$F_x = \begin{cases} \mu F_z & \text{in ploughing and cutting regimes} \\ k(A^c_{\text{atomic}})^{\xi} & \text{in no-wear, condensing, adhering and ploughing regimes} \end{cases}$$

5. The specific energy of wear is a good measure of wearability.

Acknowledgements

The authors would like to thank the continuous financial support from the Australian Research Council to this research. Dr Nicole Bordes at the Vislab of Sydney

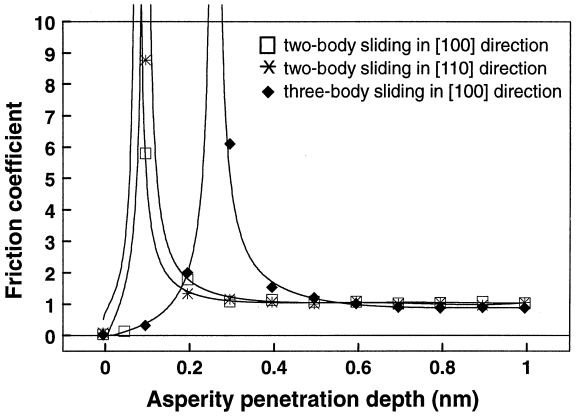

Fig. 12 Friction coefficients when sliding in different directions (V_c = 200 m/s, V_r = 100 m/s, R = 2.1 nm)

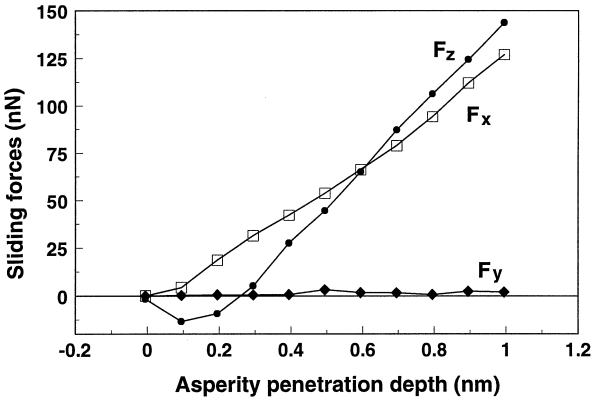

Fig. 13 Forces in three-body contact sliding processes (V_c = 200 m/s, V_r = 100 m/s, R = 2.1 nm)

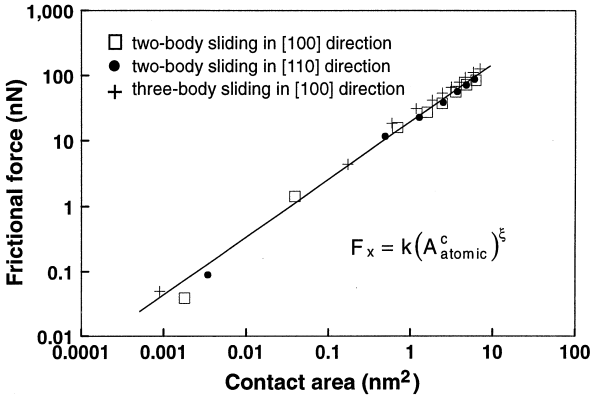

Fig. 14 Variation of frictional forces with contact area (V_c = 200 m/s, V_r = 100 m/s, R = 2.1 nm)

University helped in the data visualisation. Ms I Zarudi participated in the experimental work.

References

1. Tanaka, H. and Zhang, L. In *Advances in Abrasive Technology*, ed. L. C. Zhang and N. Yasunaga. World Scientific, Singapore, 1997, pp. 43–47.

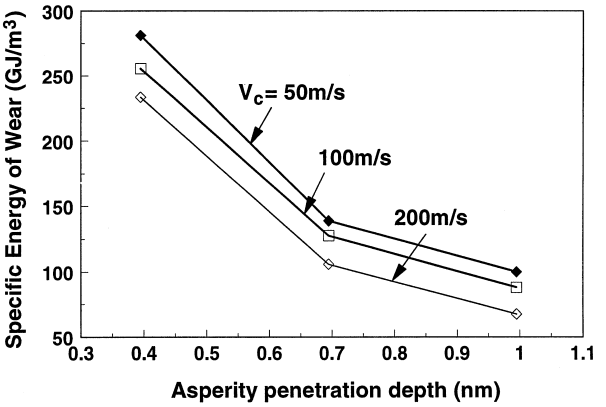

Fig. 15 Variation of specific energy of wear (R = 2.1 nm)

2. Zhang, L. and Tanaka, H., Towards a deeper understanding of friction and wear on the atomic scale: a molecular dynamics analysis. *Wear*, 1997, **211**, 44–53.
3. Zhang L. and Tanaka H. On the mechanics and physics in the nano-indentation of silicon monocrystals. *JSME International* (to appear).
4. Tersoff, J., Modelling solid-state chemistry: interatomic potential for multicomponent systems. *Physical Review B*, 1989, **39**(8), 5566–5568.
5. Hirose, K., Goto, H., Tsuchiya, H., Mori, Y., Endo, K. and Yamauchi, K., First-principles molecular dynamics simulations of material surface processing—H-termination process of Si(001) surface (in Japanese). *J. Japan Society Precision Eng*, 1994, **60**(3), 402–406.
6. Hirose, K., Goto, H., Tsuchiya, H., Mori, Y., Endo, K. and Yamauchi, K., First-principles molecular dynamics simulations of H-terminated process of Si(001) surface interacting with H_2O molecule (in Japanese). *J. Japan Society Precision Eng*, 1994, **60**(8), 1139–1143.
7. Pharr, G. M., Oliver, W. C. and Harding, D. S., New evidence for a pressure-induced phase transformation during the indentation of silicon. *J. Mater. Res.*, 1991, **6**, 1129–1130.
8. Hu, Z., Merkle, L. D., Menoni, C. S. and Spain, I. L., Crystal data for high-pressure phases of silicon. *Physical Review B*, 1986, **34**, 4679–4684.
9. Weppelmann, R., Field, J. S. and Swain, M. V., Observation, analysis and simulation of the hysteresis of silicon using ultra-micro-indentation with spherical indenters. *J. Mater. Res.*, 1993, **8**, 830–840.